

Super asymptotic giant branch stars. I – Evolution code comparison

C. L. Doherty,^{1*} L. Siess,^{1,2} J. C. Lattanzio¹ and P. Gil-Pons^{1,3}

¹Centre for Stellar and Planetary Astrophysics, School of Mathematical Sciences, Monash University, Victoria 3800, Australia

²Institut d’Astronomie et d’Astrophysique, Universit Libre de Bruxelles, CP 226, B-1050 Brussels, Belgium

³Departament de Física Aplicada, Universitat Politècnica de Catalunya, Barcelona, Spain

Accepted 2009 September 21. Received 2009 September 21; in original form 2009 June 10

ABSTRACT

We present an extensive set of detailed stellar models in the mass range 7.7–10.5 M_{\odot} over the metallicity range $Z = 10^{-5}$ –0.02. These models were produced using the Monash University version of the Mount Stromlo Stellar Structure Program (MONSTAR) and follow the evolution from the pre-main sequence to the first thermal pulse of these super asymptotic giant branch stars. A quantitative comparison is made to the study of Siess. Prior to this study, only qualitative comparisons and code validations existed in this critical mass range, and the large variations in the literature were largely unexplained. The comparison presented here is particularly detailed due to the standardization of the input physics, where possible. The minimum initial mass of star which ignites carbon, M_{up} , was found to agree within 0.2 M_{\odot} between the codes over the entire metallicity range. We find exceptional agreement in the model results between these two codes for all stages of evolution up to and including carbon burning. For additional comparison, we also present results from the EVOLVE code, a modified version of the IBEN code as described in Gil-Pons, Gutiérrez & García-Berro for some important variables during the carbon burning phase. Several numerical tests showed that the carbon burning phase is weakly dependent on the spatial resolution but that inadequate temporal resolution alters the behaviour of the convective zones. We also discovered that stars just below M_{up} may experience a carbon flash that is not followed by the development of the flame. Such aborted carbon burning models thus preserve a CO core surrounding by a 0.2–0.3 M_{\odot} shell of partially burnt carbon material. We present a simplified algorithm for calculating carbon burning that only relies on tracking two species, ^{12}C and ^{16}O , but which tests show works quite accurately for the a wide range of initial masses and compositions.

Key words: nuclear reactions, nucleosynthesis, abundances – methods: numerical – stars: AGB and post-AGB – stars: evolution.

1 INTRODUCTION

Stars in the mass range ~ 7 –11 M_{\odot} are generally referred to as super asymptotic giant branch (SAGB) stars and are the progenitors of oxygen-neon (ONe) white dwarfs and possibly the least massive neutron stars. Their evolution is unique and is characterized by the off-centre ignition of carbon under partially degenerate conditions followed by the propagation of a deflagration front towards the centre. Then, after the formation of an ONe core, the star enters the thermally pulsing SAGB phase where instabilities recurrently develop in the helium burning shell (HeBS). During this final stage of the evolution, the mass of the degenerate He-free core grows by the accretion of material from the active burning shells. The final fate of the star will then depend on whether or not the core mass

reaches the critical value of $M_{\text{EC}} \simeq 1.37 M_{\odot}$ (Nomoto 1984) above which electron capture reactions start and core collapse becomes inevitable. The outcome of the evolution is thus governed by two competing processes, namely core growth and mass loss. If the latter dominates, the envelope is removed before the core mass reaches M_{EC} and the remnant is an ONe white dwarf, otherwise the collapse of the degenerate core leads to the formation of a low-mass neutron star. The transition mass at which this division occurs has been studied in detail by several authors (Eldridge & Tout 2004; Siess 2007; Poelarends et al. 2008) and is strongly dependent on metallicity which directly impacts the mass-loss rate.

The study of the non-explosive evolution of SAGB stars started just over a decade ago in a series of papers by Garcia-Berro & Iben (1994), Ritossa, Garcia-Berro & Iben (1996), Garcia-Berro, Ritossa & Iben (1997), Iben, Ritossa & Garcia-Berro (1997) and Ritossa, Garcia-Berro & Iben (1999). In these early simulations, no mass loss was considered and a solar composition was used. Recently,

*E-mail: carolyn.doherty@sci.monash.edu.au

more models become available exploring the evolution at different metallicities (e.g. Gil-Pons & García-Berro 2002; Siess 2007) and investigating the effects of extra-mixing and binarity (Gil-Pons et al. 2005, 2007; Poelarends et al. 2008). As more and more SAGB studies populate the literature, all find qualitative similarities, despite large variations in the input physics. In particular, the mass interval of SAGB stars (which ranges between M_{up} , the minimum mass for quiescent carbon ignition and M_{mas} , the mass above which the star proceeds through all nuclear burning stages) strongly depends on the treatment of the convective boundaries (Girardi et al. 2000; Siess 2007; Poelarends et al. 2008). The existence of semiconvective layers surrounding the He burning core is responsible for variations of M_{up} by more than $3 M_{\odot}$, the value for stars of solar metallicity ranging between 6 and $9 M_{\odot}$ in different studies.

In this first paper of a series, we compare the results of computations given by two stellar evolution codes, namely Mount Stromlo Stellar Structure Program (MONSTAR) (Frost & Lattanzio 1996) and STAREVOL (Siess 2007). Each code is equipped with similar and up-to-date input physics and the simulations are started with identical initial conditions and settings concerning the composition, mass-loss rate and treatment of the convective boundaries. This allows us to concentrate on the differences caused by different implementations of numerical procedures between codes, rather than variations due to changes in input physics. This will enable us to disentangle, for example, the effects associated with extra-mixing from those related to the numerics. For additional comparison, we also present results from the EVOLVE code, a modified version of the IBEN code as described in Gil-Pons et al. (2007) for some important variables during the carbon burning phase.

In the next section, we describe the two main stellar evolution programs and the suite of MONSTAR models computed. Then, evolutionary properties of SAGB stars prior to carbon burning (Section 3) are analysed. Details about the treatment of the energetics of C burning with a limited network as in the MONSTAR code are provided in Section 4 and special attention is paid to analysing how the computation of the C burning phase depends on the space and time resolutions. Then, evolutionary properties of SAGB stars during the carbon burning phase and comparisons with STAREVOL models are presented (Section 4). Conclusions are drawn in Section 6.

2 STELLAR EVOLUTION PROGRAMS

The two main stellar evolution codes used for this study are the Monash version of the Mount Stromlo Stellar Structure Program (MONSTAR) and STAREVOL. The STAREVOL models are those detailed in Siess (2007). Recent descriptions of MONSTAR can be found in Campbell & Lattanzio (2008) and Karakas & Lattanzio (2007). The computation of SAGB models has required the implementation of carbon burning in MONSTAR and we describe later some simple approximations made to enable this modelling without increasing the number of species in the nuclear network. The opacity tables have been extended to high temperature following Campbell (2007) and Chieffi (private communication).

Given the large quantitative differences seen in previous studies of the SAGB, our main aim in this paper is a detailed comparison between our two main codes. To facilitate this, we have used, as much as possible, the same input physics and the same assumptions for some of the more contentious inputs, such as convective borders.

Common elements shared by the MONSTAR and STAREVOL codes as used in this paper are:

- (i) Strict adherence to the Schwarzschild criterion for all convective boundaries; e.g. no search for a neutrally buoyant point (such as in Lattanzio 1986) and no special treatment for semiconvection (as in an investigation of the effect of using the Ledoux criterion, see e.g. Poelarends et al. 2008).
- (ii) Standard mixing length theory (MLT) for convection with α , the mixing length parameter, set to 1.75.
- (iii) OPAL opacities (Iglesias & Rogers 1996) for $8000 \text{ K} < T < 800 \text{ MK}$, supplemented by those of Ferguson et al. (2005) at lower temperatures; conductive opacities are taken from various contributions as described in Siess (2006b).
- (iv) Neutrino losses from Itoh et al. (1996).
- (v) Electron screening factors from Graboske et al. (1973).
- (vi) Nuclear reaction rates from the NACRE compilation (Angulo et al. 1999). Note, however, that MONSTAR only accounts for seven species as opposed to STAREVOL which include 53 nuclides (see Section 4.1). Another important difference in the treatment of energy production comes from the fact that MONSTAR computes the evolution of the nuclear species at each iteration during the convergence process, while in STAREVOL it is decoupled and the nucleosynthesis is solved only once, after the structure has converged.

The major difference between the codes in relation to the input physics is the equation of state. STAREVOL uses the formalism of Pols et al. (1995) whilst MONSTAR uses a numerical integration of the Fermi–Dirac integrals.

Detailed models were calculated using MONSTAR for 23 stars in the mass range $7.7\text{--}10.5 M_{\odot}$ and with metallicities $Z = 0.02, 0.008, 0.004, 0.001, 10^{-4}$ and 10^{-5} . Initial compositions are as per Siess (2007), with all other elements taking scaled solar values assuming the Grevesse, Noels & Sauval (1996) composition. All of the stars were modelled from the zero-age main-sequence (ZAMS) through to the first thermal pulse. Mass loss is included via the Reimers prescription with $\eta = 1.0$ until carbon ignition when the Vassiliadis & Wood (1993) rate is used.

We have limited this investigation to stars which undergo partially degenerate carbon ignition, but are not massive enough to burn neon. Thus, the maximum SAGB mass M_{mas} for MONSTAR is $10.5 M_{\odot}$ compared to $10.8 M_{\odot}$ for STAREVOL. Two representative stars, the $9.5 M_{\odot} Z = 0.02$ and $9 M_{\odot} Z = 10^{-5}$ models, are chosen as case studies for our detailed comparison.

The EVOLVE models used in the carbon burning section are taken from Gil-Pons et al. (2007) and are $8.5 M_{\odot} Z = 0.02$, and 8.0 and $8.5 M_{\odot} Z = 10^{-5}$. The EVOLVE code shares the majority of the same input physics. It uses the Schwarzschild criterion for convective boundaries and has the same opacities, neutrino loss rate and initial compositions. Concerning mass loss, these models are computed with constant mass up to the SAGB phase and use the Schröder & Cuntz (2005) prescription thereafter. The nuclear burning reaction rates for hydrogen and helium use the Caughlan & Fowler (1988) compilation compared to the Angulo et al. (1999) rates used in MONSTAR and STAREVOL. We include the EVOLVE models to indicate the effect that varying the reaction rates have, and also as a further comparison for carbon burning.

3 EVOLUTION PRIOR TO CARBON BURNING

The evolutionary behaviour of intermediate mass stars (in the mass range $\approx 7\text{--}11 M_{\odot}$) prior to carbon ignition is very similar to that of lower mass stars. Both undergo convective core hydrogen burning via CNO cycling, then develop a hydrogen burning shell. For stars with metallicities $Z \geq 0.001$, they then undergo first dredge-up.

Helium ignites centrally under non-degenerate conditions, and burns in a convective core. For $Z < 0.001$, a higher central temperature leads to helium ignition before first dredge-up can occur. Upon exhaustion of central helium, the star ascends the AGB (or, more correctly, the SAGB), where carbon ignites.

The evolution of our comparison stars is shown in the Hertzsprung–Russell (HR) diagrams in Fig. 1. The log of the central density is plotted against the log of the central temperature in Fig. 2 for the pre-carbon burning phase. We find extremely close agreement between the MONSTAR and STAREVOL code results. The slight difference in the HR diagram is due to differences in the mass-loss prescription.

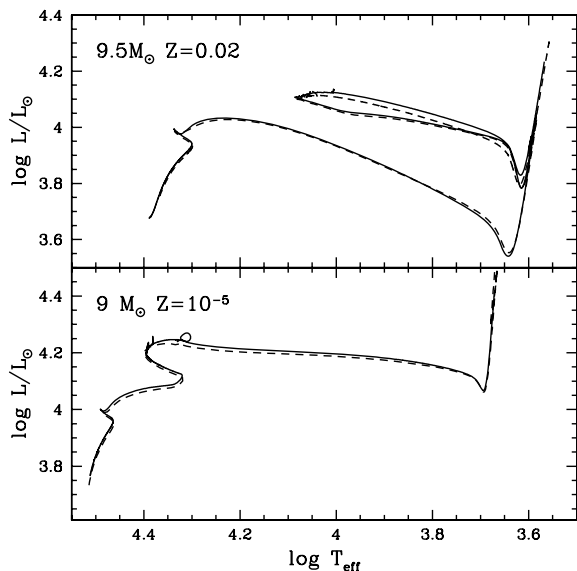


Figure 1. HR diagrams for the $9.5 M_{\odot} Z = 0.02$ and $9 M_{\odot} Z = 10^{-5}$ stellar models, until just prior to carbon ignition. Calculations with MONSTAR are shown with the solid line and those with STAREVOL use the dashed line.

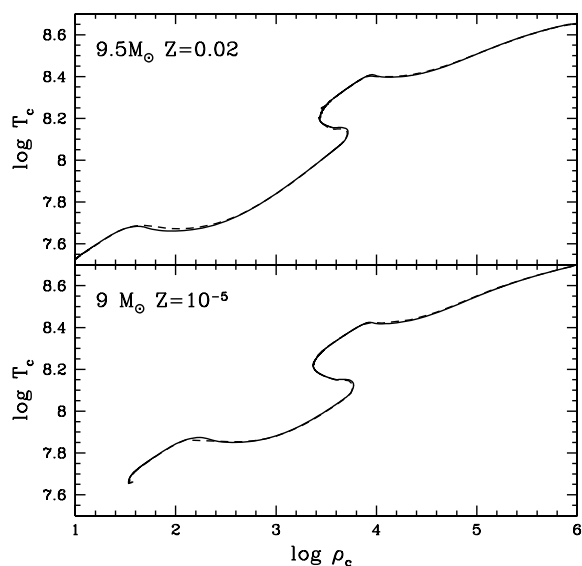


Figure 2. Log central density versus log central temperature diagram for the $9.5 M_{\odot} Z = 0.02$ and $9 M_{\odot} Z = 10^{-5}$ model stars to just prior to carbon ignition. Calculations with MONSTAR are shown with the solid line and those with STAREVOL use the dashed line.

3.1 Core hydrogen burning

The core hydrogen burning phase of evolution was found to agree very well between the two codes, as might be expected. The maximum mass of the hydrogen convective core (M_{HB}) and the duration of the core hydrogen burning phase varied by less than 2 and 4 per cent, respectively, between the two codes (for details see Table 1). The depth and time of occurrence (not shown) of the first dredge-up also compare very favourably.

3.2 Core helium burning

It is usually during the core helium burning (CHeB) phase that evolutionary codes begin to differ substantially. This is due to the presence of semiconvective layers above the helium burning core which can easily become unstable to physical or numerical perturbations (e.g. Straniero et al. 2003). The time-stepping as well as the mesh-spacing also play an important role in the modelling of this sensitive phase of evolution. In our calculations, both codes are using a strict Schwarzschild criterion for determining the convective boundaries and no extra mixing is accounted for. By standardizing our treatment of the underlying physics in this way, we minimize variations due to the use of different algorithms to handle cases where there is no neutral convective boundary, for example.

The CHeB phase can be characterized by the central temperature, the mass of the helium convective core and the central composition. The results from both codes for the $9.5 M_{\odot} Z = 0.02$ case are shown in Fig. 3. The top panel shows the time variation of the central mass fraction of the three main species: ${}^4\text{He}$, ${}^{12}\text{C}$ and ${}^{16}\text{O}$. The final values are in excellent agreement. The MONSTAR model attains a slightly higher central temperature as seen in the middle panel. This leads to an increased burning rate which results in a somewhat shorter duration of the CHeB phase (τ_{HeB}). Of particular interest is the striking similarity seen in the bottom panel between the codes for the maximum convective helium core mass at cessation of helium burning. Overall, the agreement between the codes is extremely good for such a sensitive phase of the evolution. We believe that the discrepancy between the two codes in the duration of the burning phase is due to the difference in the nuclear networks numerical effects and in particular on the use of larger time-steps in STAREVOL (see Section 5).

The situation described above is echoed throughout the metallicity range. Close agreement in the maximum convective core mass and final core abundances are found between the two codes, with the largest discrepancy between the models being the duration of the CHeB phase, which at worst is under 10 per cent (for details see Table 1). The results from EVOLVE for the CHeB phase also compare reasonably well with those of MONSTAR and STAREVOL. For instance, for the $9.5 M_{\odot} Z = 0.02$ model, the maximum size of the convective core during central helium burning is $M_{\text{HeB}} = 0.816 M_{\odot}$, that is about 5 per cent lower than the result obtained with MONSTAR, and the central carbon mass fraction at helium exhaustion is 0.305, that is about 7.5 per cent lower than the result obtained with MONSTAR. The discrepancies in this case are probably related to the use of different reaction rates (Caughlan & Fowler 1988), rather than with space and time resolution.

Note that the helium burning reaction rates between the two codes are very similar, with a maximum variation of 2 per cent in the relevant temperature range. Therefore, we do not believe that such variations determine the differences in the C mass fraction that the two codes yield at the cessation of central helium burning. Rather,

Table 1. Evolutionary characteristics prior to carbon burning.

M_{ini} (M_{\odot})	Code	M_{HB} (M_{\odot})	τ_{HB} (10^7 yr)	M_{FDU} (M_{\odot})	M_{HeB} (M_{\odot})	τ_{HeB} (10^6 yr)	X[^{12}C]	X[^{16}O]
$Z = 0.02$								
9.0	M	2.683	24.228	1.871	0.783	4.204	0.328	0.653
9.0	S	2.691	23.637	1.877	0.788	4.721	0.337	0.637
9.5	M	2.903	22.101	2.003	0.864	3.662	0.330	0.650
9.5	S	2.906	21.414	2.018	0.850	4.101	0.344	0.630
10.0	M	3.101	20.273	2.134	0.935	3.231	0.331	0.649
10.0	S	3.104	19.580	2.164	0.936	3.642	0.327	0.646
10.5	M	3.337	18.610	2.232	1.037	2.960	0.308	0.674
10.5	S	3.339	18.017	2.327	1.031	3.251	0.322	0.652
$Z = 0.008$								
8.6	M	2.650	26.500	2.215	0.763	4.393	0.356	0.636
8.6	S	2.643	27.057	2.247	0.812	4.988	0.303	0.686
9.0	M	2.804	24.703	2.298	0.854	4.032	0.327	0.665
9.0	S	2.814	23.939	2.343	0.850	4.525	0.334	0.655
9.5	M	3.029	22.254	2.384	0.937	3.633	0.316	0.676
9.5	S	3.025	21.802	2.499	0.885	3.822	0.366	0.624
10.0	M	3.254	20.696	2.401	1.040	3.234	0.316	0.676
10.0	S	3.256	20.018	2.604	1.036	3.546	0.296	0.693
$Z = 0.004$								
8.1	M	2.502	29.398	2.677	0.792	4.964	0.332	0.665
8.1	S	2.515	28.586	2.711	0.783	5.524	0.335	0.659
8.5	M	2.670	26.998	2.772	0.867	4.174	0.324	0.672
8.5	S	2.677	26.248	2.822	0.851	4.930	0.323	0.671
9.0	M	2.889	24.493	2.860	0.938	3.871	0.325	0.671
9.0	S	2.897	23.778	2.930	0.977	4.413	0.284	0.710
9.5	M	3.119	22.445	2.992	1.060	3.509	0.281	0.715
9.5	S	3.117	21.713	3.076	1.038	3.820	0.299	0.696
$Z = 0.001$								
7.7	M	2.493	31.439	7.699	0.801	4.985	0.335	0.664
7.7	S	2.460	30.630	7.685	0.771	5.354	0.364	0.634
8.0	M	2.645	29.384	7.995	0.863	4.546	0.325	0.674
8.0	S	2.611	28.637	7.984	0.864	5.068	0.304	0.695
8.5	M	2.780	26.558	8.497	0.934	3.961	0.325	0.673
8.5	S	2.793	26.841	8.484	0.931	4.234	0.313	0.686
9.0	M	3.081	24.230	8.983	1.019	3.520	0.324	0.675
9.0	S	3.020	23.440	8.983	1.023	3.830	0.317	0.682
$Z = 10^{-4}$								
8.0	M	2.665	28.690	7.998	0.867	4.345	0.326	0.674
8.0	S	2.706	28.061	7.997	0.883	4.673	0.281	0.719
8.5	M	2.978	26.067	8.498	0.935	3.780	0.330	0.670
8.5	S	2.920	25.326	8.497	0.945	4.024	0.321	0.679
9.0	M	3.111	23.621	8.998	1.030	3.406	0.313	0.687
9.0	S	3.145	23.048	8.997	1.023	3.532	0.325	0.674
$Z = 10^{-5}$								
7.7	M	2.537	30.025	7.699	0.783	4.581	0.340	0.660
7.7	S	2.530	30.251	7.698	0.761	4.662	0.348	0.652
8.0	M	2.665	28.064	7.999	0.835	4.220	0.337	0.663
8.0	S	2.668	27.613	7.998	0.855	4.536	0.319	0.681
8.5	M	2.873	25.448	8.499	0.916	3.693	0.331	0.669
8.5	S	2.875	24.962	8.498	0.910	3.912	0.331	0.669
9.0	M	3.081	23.230	8.998	0.999	3.292	0.318	0.682
9.0	S	3.110	22.749	8.998	1.013	3.490	0.317	0.683

Note. ‘M’ signifies calculation with MONSTAR whilst ‘S’ represents the STAREVOL code; M_{ini} is the initial mass; M_{HB} is the maximum convective core mass during hydrogen burning; τ_{HB} is the main sequence duration; M_{FDU} is the maximum inward extent in mass of the convective envelope during first dredge-up; M_{HeB} is the maximum mass of the convective core during helium burning; τ_{HeB} is the duration of the CHeB phase and X[^{12}C] and X[^{16}O] are the mass fractions of carbon and oxygen, respectively, in the centre at the completion of central helium burning.

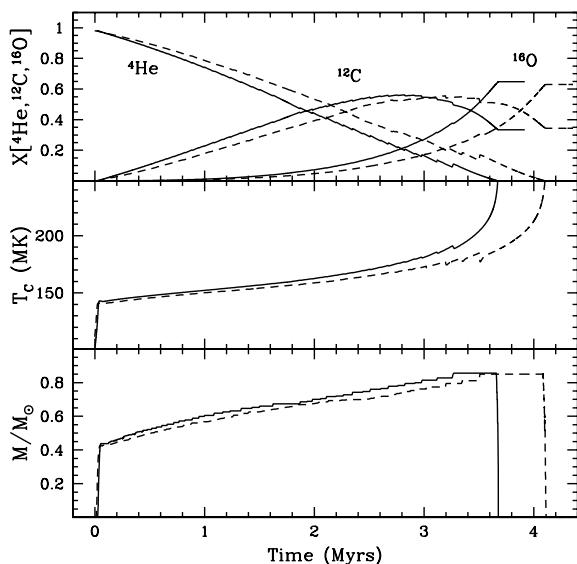


Figure 3. Evolution during CHeB showing mass fractions of ${}^4\text{He}$, ${}^{12}\text{C}$ and ${}^{16}\text{O}$ (top panel), central temperature (middle panel) and the mass of the convective helium-burning region (lower panel) for both $9.5 M_{\odot}$ $Z = 0.02$ stellar models. The time origin is set to be the start of the CHeB for both models. Calculations with MONSTAR are shown with solid lines and those with STAREVOL use dashed lines.

it is the effect of convective core breathing that determines the variations in C mass fraction. Note that the absence of any systematic trend with metallicity or mass was also found and investigated by Siess (2007).

4 COMPUTATIONAL ASPECTS OF CARBON BURNING

The carbon burning behaviour has been described in detail by Garcia-Berro & Iben (1994) and more recently by Siess (2006b), but we highlight the salient points below. After the cessation of CHeB, the stellar interior contracts, causing an increase in the central density and degeneracy with the peak temperature moving off centre. When the temperature reaches 600–650 MK, the carbon ignites. This carbon ignition, reminiscent of the core helium flash, occurs under partially degenerate conditions and is off-centre, with the ignition position (in mass) decreasing with increasing initial mass. The primary ignition is in the form of a violent flash which develops a convective shell. After quenching of the carbon flash, contraction resumes and a secondary convective zone develops (classified as a flame) which subsequently burns inwards until it reaches the centre where it extinguishes. Carbon continues to burn radiatively outwards, generating secondary convective flashes when regions of high carbon content are traversed. Carbon is not burnt to completion in the central region, with a small amount remaining (between 0.02–2 per cent), the amount dependent on the competition between the duration and temperature of the carbon burning flame (Siess 2006b). Less massive stellar models are left with more residual carbon. Overall, at the completion of carbon burning, an ONeNa core remains surrounded by an inactive carbon–oxygen shell, as well as helium and hydrogen burning shells and a large convective envelope. At the extremes of the SAGB mass range slightly different behaviour results, which we describe in Section 5.4. Before entering the detailed comparisons of our models, we first describe

a simple approximation for carbon burning that was implemented in MONSTAR.

4.1 Carbon burning reactions

The energetics of carbon burning is controlled by ${}^{12}\text{C} + {}^{12}\text{C}$ and ${}^{12}\text{C} + {}^{16}\text{O}$ reactions. In SAGB stars, the temperature does not exceed 900 MK so the contribution of the ${}^{12}\text{C} + {}^{16}\text{O}$ reactions is negligible.

The STAREVOL code models carbon burning using a detailed reaction network comprised of 53 species and in excess of 180 reactions. The MONSTAR code, however, is more computationally expedient, limiting the reaction network to a small number of species (H , ${}^3\text{He}$, ${}^4\text{He}$, ${}^{12}\text{C}$, ${}^{14}\text{N}$, ${}^{16}\text{O}$, Z_{Other}) and including only the most energetic, and therefore structurally important, nuclear reactions. Because detailed nucleosynthesis is performed using a separate post-processing code, MONSOON (Cannon 1993; Lugaro et al. 2004), we did not feel it necessary to increase the number of species or reactions in MONSTAR so long as the energetics are correctly modelled. We are aware that the limited carbon burning network in our evolutionary code will not produce the details of core composition, however, this will be achieved after post-processing. We approximate carbon burning through the use of a single overall reaction and corresponding reaction rate to encompass all the energetically important primary and secondary reactions.

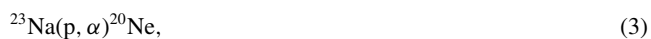
The two most active primary carbon burning channels are the ${}^{12}\text{C}({}^{12}\text{C}, \text{p}){}^{23}\text{Na}$ and ${}^{12}\text{C}({}^{12}\text{C}, \alpha){}^{20}\text{Ne}$ reactions, which occur at almost the same rate (Caughlan & Fowler 1988). Previously, the MONSTAR code has used the ‘no sodium’ approximation where the protons produced by ${}^{12}\text{C} + {}^{12}\text{C}$ were assumed to be instantaneously reabsorbed by ${}^{23}\text{Na}$ undergoing the reaction ${}^{23}\text{Na}(\text{p}, \alpha){}^{20}\text{Ne}$. This reduced the two major channels to just the ${}^{12}\text{C}({}^{12}\text{C}, \alpha){}^{20}\text{Ne}$ reaction. The α particles from the above reaction were assumed to be absorbed by ${}^{16}\text{O}$ via ${}^{16}\text{O}(\alpha, \gamma){}^{20}\text{Ne}$. This resulted in the overall reaction ${}^{12}\text{C} + {}^{12}\text{C} + {}^{16}\text{O} \rightarrow 2 {}^{20}\text{Ne} + 2\gamma$, with the energy generation rate Q per ${}^{12}\text{C}$ pair for this overall reaction of 9.355 MeV. This is the lowest possible Q value, as the products all proceed to ${}^{20}\text{Ne}$.

Due to the intricate carbon burning behaviour in SAGB stars, a more thorough exploration of the carbon burning approximation was required, focusing on the secondary reactions involving the protons and alpha particles. A significant obstacle to a one-reaction carbon burning network is the time dependence of the variable composition in the carbon burning region, for both the flashes and flames. Indeed, as carbon burning proceeds, the composition of the burning shell becomes more complex, including the ashes of He burning, mainly ${}^{12}\text{C}$, ${}^{16}\text{O}$ and trace amounts of ${}^{22}\text{Ne}$ and ${}^{25,26}\text{Mg}$, but also the products of C-burning, namely ${}^{20}\text{Ne}$, ${}^{23}\text{Na}$ and ${}^{24}\text{Mg}$.

We have approximated the carbon burning reactions in the following way. Each reacting pair of ${}^{12}\text{C}$ nuclei are assumed to follow either of two paths with equal (50 per cent) probability:



Now we consider the fate of the products on the right-hand side. First, for ${}^{23}\text{Na}$, there are two dominant channels at these temperatures:

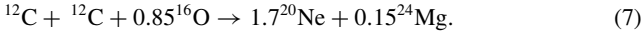


To allow for the temporal variation of temperature and abundance, we assume 85 per cent of the sodium follow the (p, α) channel and

15 per cent follows the (p,γ) route. This removes all sodium and protons from the reactions and we have to follow the fate of the α particles. Again, noting the dominant rates and species present, we assume 92 per cent of the α s react with ^{16}O and only 8 per cent with ^{20}Ne in the reactions:



Collecting all of these reactions, we end up with the single composite reaction of



Including the Q values for all reactions gives us a total $Q = 10.0$ MeV for this composite reaction. Note that this allows one to calculate the entire carbon burning evolution, to good accuracy, by including only two species, ^{12}C and ^{16}O .

We are aware that at the higher end of the temperature regime ($T \geq 850$ MK), we are overestimating the Q value by assuming a larger fraction follows the more energetic path to ^{24}Mg . However, as the majority of carbon burning takes place below this temperature, we are confident that this overestimate does not affect the results significantly. To test the effect of the energetics of the carbon burning network, models were run with Q values of 9.355, 10 and 10.5 MeV for the $9.5 M_{\odot} Z = 0.02$ case. The changes to the flash/flame morphology due to variation in Q were minor, with an increased Q value leading only to a 5 per cent increase in the duration of the carbon burning flame. As extra energy is injected into the star when Q is greater, the convective region extends further outwards in mass and mixes in more fresh carbon, leading to a slightly longer lived flame. A comparable, or possibly larger effect, is that the higher Q value produces a lower temperature and hence a lower neutrino luminosity. This effect also adds to the longer duration of carbon burning. The maximum carbon burning luminosity during the primary flash $L_{C_{\text{flash}}}$ shows negligible variation.

The rate of the overall carbon reaction chain is set by the slowest reaction, in this case the $^{12}\text{C}(^{12}\text{C}, p)^{23}\text{Na}$ reaction. The dependence of the carbon burning behaviour on the rate of the $^{12}\text{C} + ^{12}\text{C}$ reactions was seen to play a minor role by Siess (2006b). We note, however, that a change to the carbon burning reaction rate will effect $L_{C_{\text{flash}}}$, with a lower carbon burning rate leading to a more violent and luminous flash, since higher temperatures will be reached. A slower carbon burning rate also affects the central conditions, with an increased density and decreased temperature at carbon ignition.

We also tested the effect of varying the proportion of ^{16}O reacting and hence the relative production of ^{20}Ne relative to ^{24}Mg . The composition of the cores was slightly altered but the effects on the flame/flash morphology and luminosity of the primary carbon flash were negligible.

Although the details of the changes in flash/flame morphology are of interest, more important is the effects that modest variations in Q , reaction rate or product abundance have on the carbon–oxygen (CO) core mass, fraction of unburnt carbon and depth of second dredge-up (2DUP). These quantities dictate the stars' further evolution and the nature of their subsequent demise. In all test models, these variables are barely affected with, at maximum, less than 1 per cent variation in both the CO core mass and depth of 2DUP and a 4 per cent variation in the mass fraction of ^{12}C remaining. This shows the robustness of our simple implementation of carbon burning.

4.2 Spatial and temporal resolution

Timmes, Woosley & Taam (1994), and more recently Garcia-Berro et al. (1997) and Siess (2006b) have suggested that to adequately model the convective carbon burning behaviour, in particular the flame propagation to the centre, extremely stringent temporal and spatial resolution is required. In MONSTAR, these resolutions are determined by placing constraints on the changes in mass, luminosity, pressure, temperature, radius and composition between mesh-points. Our usual spatial constraints are:

- (i) $\Delta m/M < 0.02$,
- (ii) $\Delta L/L_{\odot} < 0.2$,
- (iii) $\Delta \ln T < 0.2$,
- (iv) $\Delta \ln P < 0.2$,
- (v) $\Delta r/R_{\odot} < 0.2$,
- (vi) $\Delta X_i < 0.1$ and
- (vii) $\Delta \ln X_i < 7.5$,

where the differences are between adjacent mesh-points. We also constrain the fractional change in the abundance of species i between two mass shells j and $j + 1$ to be

$$1/f < \left| X_i^j/x_i^{j+1} \right| < f \quad (8)$$

with $f = 7.5$.

The temporal resolution is determined by analogous relations for the variables at the same mesh-point between consecutive models:

- (i) $\Delta \ln T < 0.15$,
- (ii) $\Delta \ln P < 0.15$,
- (iii) $\Delta X_i < 0.15$ and
- (iv) $\Delta \ln X_i < 0.8$.

We supplement this with conditions on the change in luminosity given by

- (i) $\Delta \ln L_H < 0.15$,
- (ii) $\Delta \ln L_{\text{He}} < 0.15$ and
- (iii) $\Delta \ln L_C < 0.15$

where the differences are taken between consecutive models.

To find the most appropriate resolution, a series of test models were run with the settings above divided by a factor F_{space} for the spatial variations and a factor F_{time} for the time variations (our standard case, obviously, has $F_{\text{space}} = F_{\text{time}} = 1$). We ran test cases with our usual resolution as well as with these constraints tightened by factors of 2 and 4 ($F_{\text{space}} = 1, 2, 4, F_{\text{time}} = 1, 2, 4$), giving nine cases in total.

During carbon burning the mesh spacing is dictated primarily by the luminosity restrictions, whilst the time-step is driven by the pressure and temperature restrictions. When $F_{\text{time}} = 1$ and $F_{\text{space}} = 1, 2$ or 4, the resulting flash/flame morphology is the same and consists of three primary flashes and a flame. However, when $F_{\text{space}} = 1$ and with increased time resolution ($F_{\text{time}} = 2$ or 4), the convective behaviour changed, then consisting of one primary flash and a flame. For the most stringently resolved case (when $F_{\text{space}} = F_{\text{time}} = 4$), the convective behaviour also consisted of one primary flash and a flame. This suggests that the time-step must be sufficiently short for carbon burning convective behaviour to be adequately modelled, given an adequate spatial resolution.

The MONSTAR carbon burning temporal and spatial standard/default resolutions chosen for our calculations were $F_{\text{space}} = F_{\text{time}} = 2$, which produces resolution finer than that recommended by Timmes et al. (1994). The models contain between 1500 and

2000 mesh shells and time-steps between $2 \times 10^{-2} - 50$ yr in the carbon burning phase. This compares well with Siess (2006b) whose mesh spacing is dictated by a 10 per cent variation in luminosity and other variables.

We note that, although the flash/flame morphology is considerably different with differing temporal resolutions, the most important global properties for the subsequent evolution, such as core composition, depth of 2DUP and core mass show negligible variations, within 4 per cent for the remaining core carbon content and less than 1 per cent in the mass of the core.

5 COMPARISON OF THE RESULTS OF THE CARBON BURNING PHASE

Here, we present a detailed comparison between the MONSTAR and STAREVOL code results, focusing on our two illustrative stars, the $9.5 M_{\odot} Z = 0.02$ and the $9 M_{\odot} Z = 10^{-5}$ models, for the carbon burning phase until the first thermal pulse. We also compare the results from three EVOLVE stellar models, for the carbon ignition position.

In all models, carbon ignites at degeneracy $\psi \approx 2.7$, temperature ≈ 640 MK and density $\approx 10^6$ g cm $^{-3}$. The contraction time from the cessation of the CHeB until the first convective carbon ignition $\tau_{\text{CB-HeB}}$ are detailed in Table 2 and show remarkable similarity.

Fig. 4 shows the evolution of a selection of characteristics during the carbon burning phase for both codes for the $9.5 M_{\odot} Z = 0.02$ star. The primary carbon flash can be identified by the sharp peak in L_C in the top panel which also includes the behaviour of the helium (L_{He}), hydrogen (L_{H}) and neutrino (L_{ν}) luminosities. The luminosity of the flashes and flames vary slightly between the codes, with the primary flash more intense in the STAREVOL model. The next panel highlights the similarity in the convective behaviour; the relative positions of events in time as well as the depth of the 2DUP are both very similar. The positions of first ignition in mass, m_{ign} and corresponding CO core mass, defined as point of maximum energy generation by helium burning, are 0.513 and $1.122 M_{\odot}$ in MONSTAR compared to 0.534 and $1.095 M_{\odot}$ in STAREVOL. Despite having comparable convective core masses at the end of helium burning and very similar contraction times between the end of central helium burning and the onset of carbon burning ($\tau_{\text{CB-HeB}}$, see Table 2), by the time of carbon ignition the CO core masses between the models have diverged, with the MONSTAR model systematically retaining a slightly more massive CO core (a few per cent). The cause of this divergence is MONSTAR burning He faster, which leads to a higher core growth rate. This effect was also seen when comparing the duration of core He burning. Although the rates for the 3α and $^{12}\text{C}(\alpha, \gamma)$ rates are almost identical between the codes, MONSTAR always burns helium more efficiently compared to STAREVOL. The origin of this difference is hard to trace as many factors contribute to modify the thermal structure of the helium burning region, including the space and time resolutions which are different between the codes. However, when a further model was computed using the STAREVOL code with a much finer time resolution during the contraction phase, $\tau_{\text{CB-HeB}}$ was seen to increase from 2.373 to 2.444×10^5 yr. This increased contraction time led to a larger CO core at carbon ignition, $1.125 M_{\odot}$ compared to $1.095 M_{\odot}$ previously. This STAREVOL core mass now closely matches the $1.122 M_{\odot}$ found with MONSTAR. We conclude that the differences appearing during core He burning are due to larger time-steps usually taken in the STAREVOL code, and a small reduction in this would

bring the codes into even closer agreement during this demanding phase.

The second bottom panel of Fig. 4 depicts the evolution of both central temperature and maximum temperature with time. Here, we see that the maximum temperature in the STAREVOL models is slightly greater which leads to faster carbon burning as the flame speed is proportional to T^{14} (Timmes et al. 1994). Lastly, the bottom panel of this figure shows the close agreement of the stellar radius and surface luminosity. Overall the agreement between the two codes is excellent.

Fig. 5 shows profiles of some relevant variables at different times during the carbon burning phase of evolution of the $9.5 M_{\odot} Z = 0.02$ star. These profiles show close agreement in the three plotted variables but for the slight difference in the core mass. We also note that carbon is depleted more rapidly in STAREVOL but the final core composition is very similar.

Examination of the central conditions (Fig. 6) indicates that the point of ignition varies between the codes, with the MONSTAR models igniting at slightly higher temperature and lower density. When the flame reaches the centre, the MONSTAR models show comparable temperatures but are at a lower density. These modest differences are attributed to the high dependence of the central conditions on the carbon burning reaction rate as well as both spatial and temporal resolutions, and also on differences in core mass. To test the effect of the difference in CO core mass, we have also compared a $9.3 M_{\odot}$ MONSTAR model which has a CO core mass comparable to the $9.5 M_{\odot}$ STAREVOL model. We can see the close similarity of the $T_c - \rho_c$ evolution during the main carbon burning phase until the central temperature suddenly jumps above 4×10^8 K when the flame reaches the centre. The differences shown in the Fig. 6 after that moment can be ascribed to some numerical effects (time and space resolution), but these small differences have no impact on the subsequent evolution.

As illustrated in Fig. 7, the differences between the $9 M_{\odot} Z = 10^{-5}$ models are again minimal. Starting with an initially more massive CO core, the 2DUP is postponed to near the end of carbon burning and unlike the $9.5 M_{\odot} Z = 0.02$ case, hydrogen does not reignite during the flame's propagation to the centre. Another point of interest is the smaller temperature range in the core. There is a slight difference between the speeds of the convective envelopes' inward penetrations.

The duration of the carbon burning¹ is a decreasing function of the CO core mass which depends on initial metallicity and stellar mass. As indicated in Table 2, the carbon burning duration in the MONSTAR models is longer by ≈ 15 per cent for models of the same initial mass. The most likely cause of this difference is the interplay of slight differences in the carbon burning energy generation rate and resolution. As the overall carbon burning phase of evolution is very short ($< 40\,000$ yr), the variation in duration is of negligible importance to further evolution. The duration of the carbon burning phase shows no direct dependence on initial metallicity at a given core mass.

In the more metal-rich stellar models, the stellar mass at carbon ignition, M_{CB} , varies between the two codes with the MONSTAR model consistently more massive. This discrepancy is primarily due to the shorter duration of helium burning in the MONSTAR models reducing the total mass lost. In the lower metallicity models, this difference is negligible as the mass loss is less efficient.

¹ Defined here from the first carbon flash to first thermal pulse.

Table 2. Carbon burning characteristics.

M_{ini} (M_{\odot})	Code	$\tau_{\text{CB-HeB}}$ (10^5 yr)	M_{CB} (M_{\odot})	M_{CO_i} (M_{\odot})	m_{ign} (M_{\odot})	$L_{\text{C}_{\text{flash}}}$ (L_{\odot})	M_{SDU} (M_{\odot})	M_{SAGB} (M_{\odot})	M_{ONe} (M_{\odot})	M_{CO} (M_{\odot})
$Z = 0.02$										
9.0	M	2.918	8.819	1.078	0.665	1.139 (8)	1.097	8.715	1.051	1.099
9.0	S	2.918	8.793	1.053	0.839	4.558 (8)	1.060	8.788	1.043	1.063
9.5	M	2.409	9.312	1.122	0.513	1.796 (7)	1.162	9.272	1.146	1.162
9.5	S	2.379	9.277	1.095	0.534	3.838 (7)	1.123	9.219	1.108	1.125
10.0	M	1.938	9.801	1.183	0.366	6.295 (6)	1.210	9.791	1.181	1.201
10.0	S	1.889	9.757	1.164	0.394	1.371 (7)	1.188	9.741	1.182	1.188
10.5	M	1.506	10.329	1.247	0.229	2.802 (6)	1.294	10.301	1.267	1.267
10.5	S	1.510	10.233	1.246	0.249	5.895 (6)	1.256	10.226	1.246	1.252
$Z = 0.008$										
8.6	M	2.733	8.437	1.062	0.788	1.023 (8)	1.071	8.436	1.037	1.076
8.6	S	2.761	8.422	1.059	0.855	8.303 (8)	1.060	8.421	1.053	1.053
9.0	M	2.389	8.765	1.121	0.519	1.917 (7)	1.160	8.752	1.142	1.160
9.0	S	2.409	8.807	1.084	0.597	4.346 (7)	1.109	8.800	1.090	1.110
9.5	M	1.952	9.353	1.180	0.397	6.770 (7)	1.219	9.334	1.181	1.210
9.5	S	2.179	9.291	1.126	0.472	1.855 (7)	1.159	9.281	1.150	1.159
10.0	M	1.534	9.896	1.260	0.224	2.708 (6)	1.295	9.862	1.288	1.295
10.0	S	1.492	9.797	1.247	0.275	6.713 (6)	1.257	9.793	1.246	1.252
$Z = 0.004$										
8.1	M	2.937	8.025	1.078	0.665	1.170 (8)	1.097	8.022	1.065	1.098
8.1	S	3.014	8.023	1.058	0.839	1.870 (8)	1.064	8.021	1.048	1.064
8.5	M	2.346	8.424	1.125	0.511	1.780 (7)	1.168	8.423	1.137	1.168
8.5	S	2.416	8.417	1.097	0.580	3.382 (7)	1.123	8.411	1.107	1.124
9.0	M	1.928	8.921	1.179	0.366	6.533 (6)	1.221	8.907	1.203	1.222
9.0	S	1.730	8.908	1.189	0.377	9.149 (6)	1.202	8.902	1.197	1.203
9.5	M	1.447	9.418	1.268	0.222	2.719 (6)	1.298	9.397	1.292	1.298
9.5	S	1.503	9.401	1.253	0.265	6.601 (6)	1.276	9.398	1.244	1.258
$Z = 0.001$										
7.7	M	2.856	7.684	1.087	0.618	6.153 (7)	1.110	7.684	1.073	1.110
7.7	S	3.238	7.684	1.058	0.826	5.533 (8)	1.066	7.684	1.047	1.069
8.0	M	2.387	7.984	1.117	0.520	1.808 (7)	1.168	7.984	1.137	1.168
8.0	S	2.373	7.984	1.103	0.563	3.302 (7)	1.129	7.984	1.113	1.128
8.5	M	1.976	8.482	1.175	0.397	6.625 (6)	1.220	8.482	1.202	1.219
8.5	S	1.998	8.483	1.159	0.424	1.806 (7)	1.185	8.480	1.179	1.195
9.0	M	1.599	8.983	1.248	0.233	3.016 (6)	1.287	8.983	1.271	1.285
9.0	S	1.604	8.983	1.243	0.272	5.229 (6)	1.256	8.982	1.244	1.251
$Z = 10^{-4}$										
8.0	M	2.365	7.997	1.131	0.492	1.502 (7)	1.178	7.996	1.163	1.179
8.0	S	2.260	7.997	1.119	0.548	2.604 (7)	1.142	7.996	1.128	1.141
8.5	M	1.961	8.497	1.187	0.365	5.874 (6)	1.229	8.497	1.217	1.230
8.5	S	1.942	8.497	1.177	0.394	9.985 (6)	1.196	8.496	1.191	1.197
9.0	M	1.574	8.997	1.255	0.235	2.861 (6)	1.292	8.997	1.286	1.292
9.0	S	1.635	8.997	1.248	0.253	6.792 (6)	1.277	8.996	1.242	1.256
$Z = 10^{-5}$										
7.7	M	2.985	7.699	1.087	0.617	5.938 (7)	1.096	7.699	1.066	1.097
7.7	S	3.344	7.698	1.057	0.814	3.752 (8)	1.066	7.698	1.043	1.068
8.0	M	2.551	7.999	1.120	0.515	1.848 (7)	1.167	7.999	1.150	1.169
8.0	S	2.488	7.998	1.104	0.561	3.153 (7)	1.131	7.998	1.116	1.132
8.5	M	2.047	8.499	1.175	0.383	6.708 (6)	1.220	8.499	1.195	1.219
8.5	S	2.148	8.498	1.139	0.426	1.818 (7)	1.185	8.498	1.179	1.186
9.0	M	1.672	8.999	1.243	0.260	3.279 (6)	1.292	8.999	1.282	1.292
9.0	S	1.666	8.998	1.239	0.280	7.209 (6)	1.258	8.998	1.239	1.249

Note. ‘M’ signifies calculation with MONSTAR whilst ‘S’ represents the STAREVOL code. M_{ini} is the initial mass; $\tau_{\text{CB-HeB}}$ is the contraction time defined as the time between the end of central He burning and C-ignition; M_{CB} is the total mass at carbon ignition, M_{CO_i} is the carbon–oxygen core mass at the time of the primary carbon flash; m_{ign} is the mass of base of the first convective flash; $L_{\text{C}_{\text{flash}}}$ is the maximum carbon luminosity during the flash; M_{SDU} is the maximum depth of the 2DUP; M_{SAGB} is the total stellar mass at the first thermal pulse; M_{ONe} is the ONe core mass at the first thermal pulse; M_{CO} is the mass of the CO core at the first thermal pulse.

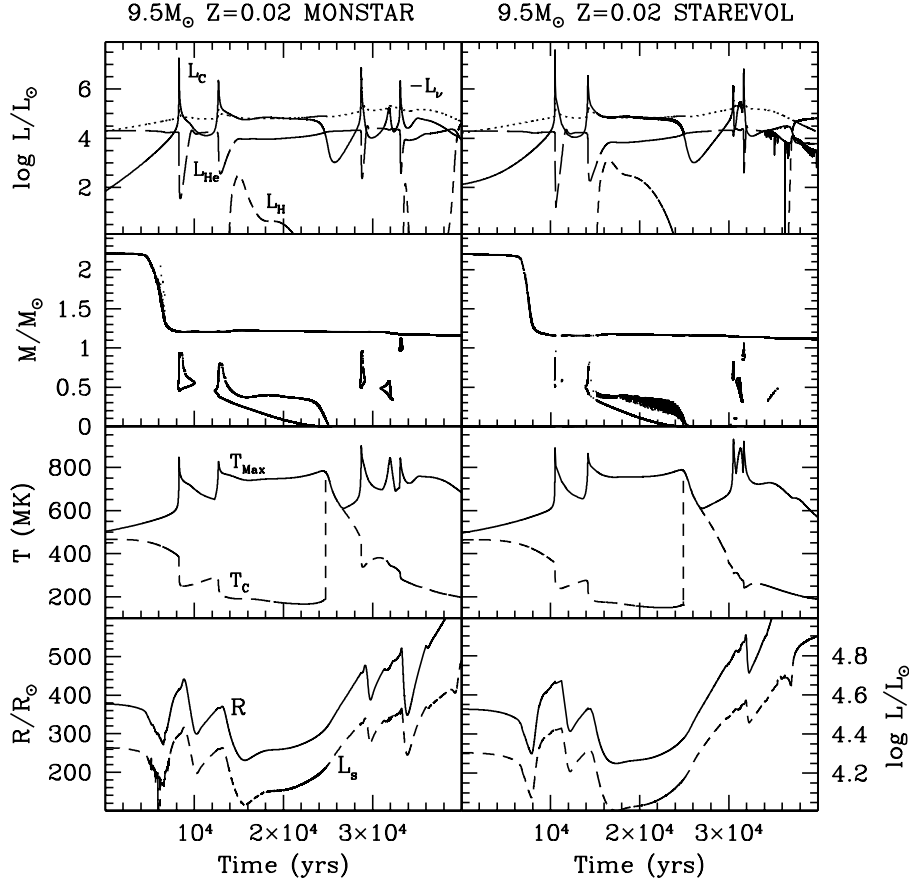


Figure 4. Carbon burning characteristics for $9.5 M_{\odot}$ $Z = 0.02$ models. From the top to bottom, we have: evolution of the carbon, helium, hydrogen and neutrino luminosities with time; Kippenhahn diagram shown with the convective carbon burning flash and flame characteristics and the base of the convective envelope; maximum and central temperatures and stellar radius and surface luminosity. The time axis has been offset to begin when L_C exceeds $100 L_{\odot}$.

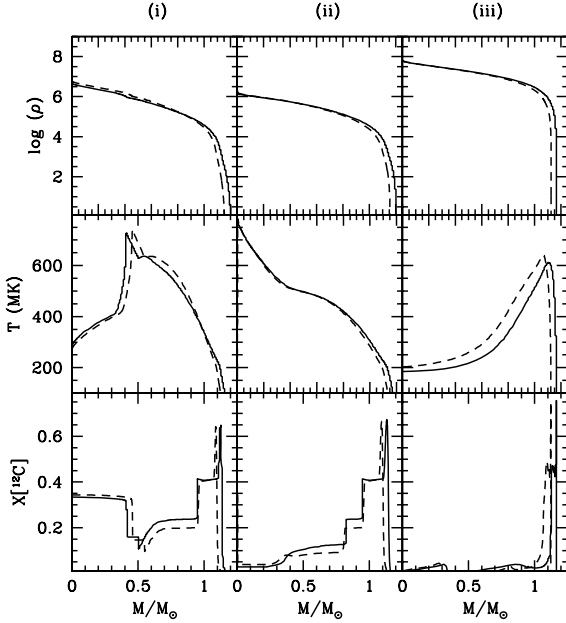


Figure 5. Selected variables as a function of mass for the inner regions of the $9.5 M_{\odot}$ $Z = 0.02$ model during (i) the primary convective flash, (ii) just after the convective flame has reached the centre and (iii) just after cessation of carbon burning. The panels display, from the top to bottom, log density, temperature and carbon mass fraction. Calculations with MONSTAR are shown with the solid line and those with STAREVOL use the dashed line.

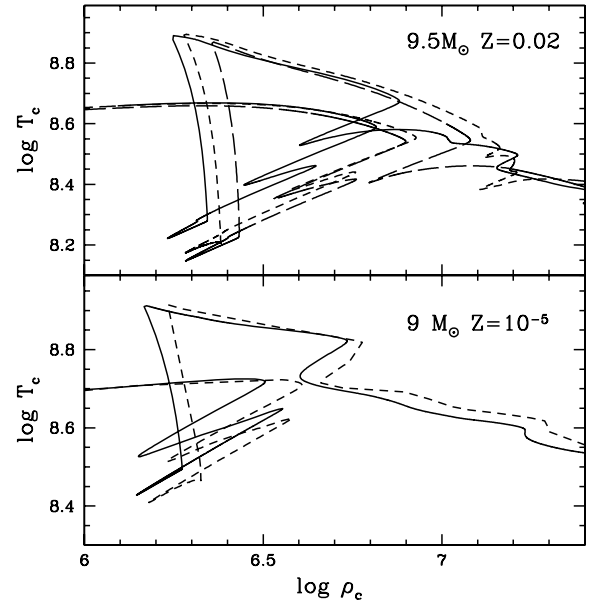


Figure 6. Log central density versus log central temperature diagrams for the $9.5 M_{\odot}$ $Z = 0.02$ and $9 M_{\odot}$ $Z = 10^{-5}$ models during the carbon burning phase of evolution. Calculations with MONSTAR are shown with the solid line and those with STAREVOL use the dashed line. In the top panel, a $9.3 M_{\odot}$ $Z = 0.02$ MONSTAR model is included with long-dashed lines. The temperature axis is more extended for the $9.5 M_{\odot}$ $Z = 0.02$ models.

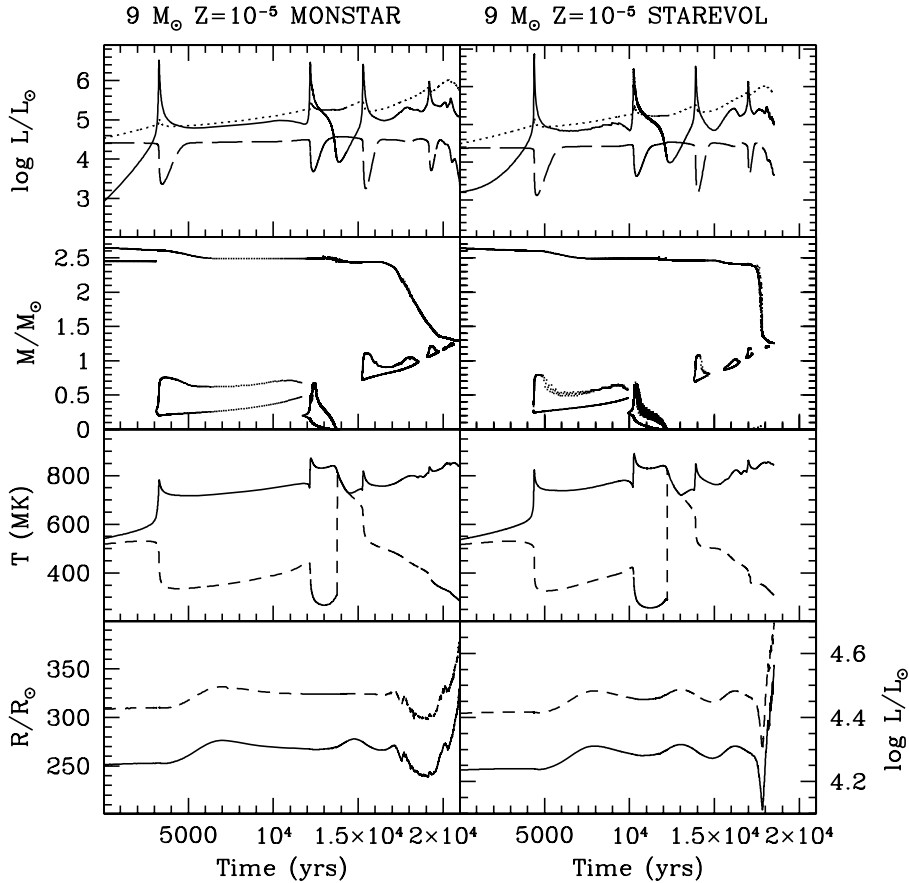


Figure 7. As in Fig. 4, but for $9 M_{\odot} Z = 10^{-5}$ models. Note the changes in scale of the radius/surface luminosity and temperature plots.

5.1 M_{up} values

An important quantity determining the ultimate fate of the star is the minimum initial mass M_{up} above which carbon ignites. This value varies greatly between authors, ranging from 6 to $9 M_{\odot}$ for solar composition models (e.g. Siess 2007). Over the metallicity range discussed in this study, the MONSTAR and STAREVOL codes have a difference in M_{up} of $\approx 0.2 M_{\odot}$, with the M_{up} value consistently lower in the MONSTAR models. This is again a consequence of MONSTAR having larger core masses at carbon ignition as a result of a faster helium burning rate. In any event, the differences here are usually swamped by different ways of calculating the burning and mixing during CHeB.

5.2 Ignition conditions

In Fig. 8, we plot the ignition position m_{ign} (in M_{\odot}) and the maximum carbon burning luminosity achieved during the primary flash L_{Cflash} versus CO core mass for all computed models using MONSTAR and STAREVOL. We also include model results from the EVOLVE code for three stellar models, sufficient to populate the entire core mass range. Excellent agreement between the m_{ign} values is found in all three codes' results.

From the top panel of Fig. 8, we deduce that for a given core mass the ignition position does not depend on the initial metallicity since all the points follow the same relation and also that $m_{\text{ign}} \lesssim 0.8 M_{\odot}$ for both codes, a result also found by Timmes et al. (1994) and Poelarends et al. (2008).

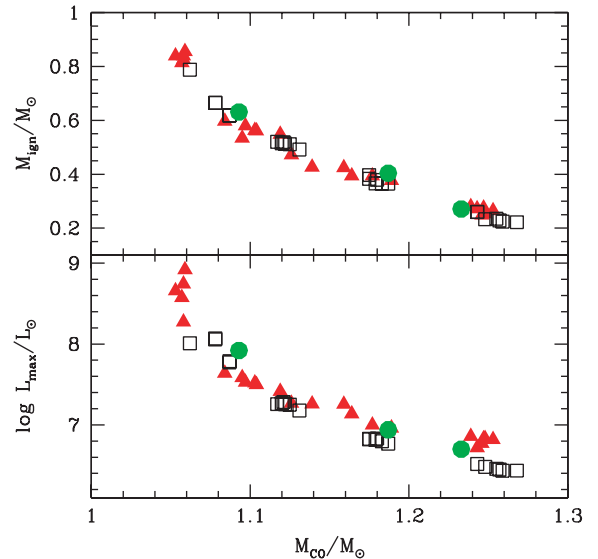


Figure 8. Ignition conditions; CO core mass versus ignition position in mass for the first flash m_{ign} (top) and maximum carbon burning luminosity achieved during the primary flash (bottom). Calculations with MONSTAR are shown with open squares, STAREVOL use the filled triangles and EVOLVE models are shown with filled circles.

This study has only included stellar models which have experienced an efficient 2DUP which has reduced the core mass to below the Chandrasekhar limit. Models which ignite carbon more centrally ($m_{\text{ign}} \lesssim 0.2 M_{\odot}$) avoid the 2DUP and will evolve as massive stars through all the nuclear burning stages.

The bottom panel of Fig. 8 shows the close agreement of $L_{C_{\text{flash}}}$ with the differences between the STAREVOL and MONSTAR code increasing in the higher core mass range where $M_{\text{CO}} > 1.24 M_{\odot}$. As found in Section 4.1, a modest change in carbon reaction rate can change the flash luminosity $L_{C_{\text{flash}}}$, with a slower rate leading to a more violent (luminous) flash.

Given that the position in mass of carbon ignition is dependent not only on the equation of state, neutrino losses and energy generation rates, but also a range of other contributing factors, the extreme similarity between the three code results here, tend to indicate that there exists a kind of universal relation between these quantities.

5.3 Second dredge-up

As found by Garcia-Berro et al. (1997), the stage of evolution when the 2DUP occurs in SAGB stars changes with initial mass. In lower mass SAGB stars, it is prior to carbon burning; while in the massive SAGB stars, it occurs after cessation of carbon burning. As discussed in Siess (2007) and Poelarends et al. (2008), massive stars avoid the 2DUP and therefore keep massive H-free cores. The presence of the 2DUP is thus of uttermost importance for the subsequent evolution of the star as it decreases its core mass below the Chandrasekhar limit. Poelarends et al. (2008) found, using the STERN (Langer 1998; Heger, Langer & Woosley 2000) and EVOL (Blöcker 1995; Herwig 2000) codes that the depth of the 2DUP forms a distinct discontinuity between models which have efficient 2DUP and those that do not experience 2DUP at all. No models are left with core masses between ≈ 1.4 – 2.6 . We find this discontinuity in depth of 2DUP in both MONSTAR and STAREVOL codes. Comparison of the numbers in Table 2 again shows a very good agreement between the codes concerning the depth and position in time of 2DUP.

5.4 Low- and high-mass SAGB stars – aborted carbon burning and dredge out

In the very lowest mass SAGB models, carbon ignition occurs within the outer $\approx 0.2 M_{\odot}$ of the CO core. Due to this far off-centre ignition, only a very brief primary carbon flash results. When this flash is extinguished, carbon burning ceases entirely. These models are left with a CO core surrounded by a ≈ 0.2 – $0.3 M_{\odot}$ shell comprising material that has undergone only partial carbon burning.

For example, an $8.75 M_{\odot}$ $Z = 0.02$ MONSTAR model shows this aborted carbon ignition (and is hence not defined as a SAGB star). The CO core mass at ignition is $1.058 M_{\odot}$ and the ignition occurs at m_{ign} of $0.799 M_{\odot}$. The initial flash is quite violent with a luminosity maximum $L_{C_{\text{flash}}}$ of $2.519 \times 10^8 L_{\odot}$. This is only slightly more energetic than other MONSTAR models, which go on to burn carbon completely. The duration of the flash is only 370 yr. After the carbon burning ceases, this model is left with a CO core only slightly less massive than stars which do complete carbon burning, such as the $8.6 M_{\odot}$ $Z = 0.008$ model which has a CO core mass of $1.062 M_{\odot}$.

The ignition conditions (such as the density, degeneracy and temperature) in these cases are not clearly distinguishable from the more massive stellar models which do burn carbon. We note that

some STAREVOL models have CO core masses less than $1.058 M_{\odot}$ but undergo complete carbon burning. This suggests that the core mass boundary for aborted carbon ignition can be affected by temporal and spatial resolution, as well as the carbon burning rate. Aborted carbon ignition occurs over a very small mass range $< 0.2 M_{\odot}$ below M_{up} .

On the other hand, the most massive SAGB star models undergo a ‘dredge out’ event (Iben et al. 1997; Siess 2006a). Near the cessation of carbon burning, the massive ONe core is contracting and releases large amounts of gravitational energy which heat up the He-rich layers. The temperature increase induces the development of a convective instability in the helium shell which grows in mass and eventually meets the inward-moving convective envelope.

In this study, the only model that underwent a dredge out event was the STAREVOL $10 M_{\odot}$ $Z = 0.008$ model. Determining which models will show a dredge out event is not strictly a function of the core mass. This is seen in Table 2 where STAREVOL models with more massive CO cores (e.g. $9.5 M_{\odot}$ $Z = 0.004$) and comparable total masses do not undergo dredge out events. No MONSTAR models included in this study undergo dredge out events. The reason for this is that dredge out in MONSTAR models occurs in slightly more massive cores (and initial stellar masses $\approx 0.2 M_{\odot}$ greater) than the STAREVOL models, and hence larger than included in this study. Due to this, and the lower M_{Up} value obtained, the MONSTAR code SAGB models cover a larger initial mass range by $\approx 0.4 M_{\odot}$. We note here that the temporal and spatial resolutions near the end of carbon burning are important in these massive SAGB models as the intensity and duration of the secondary carbon flashes (which can be modified by changes in resolution) feed the interplay between the gravitational and nuclear burning luminosities that causes a dredge out event. A thorough exploration of the evolution and nucleosynthesis that occur in SAGB star models at the extremes of the mass range will be described in a forthcoming paper in this series.

5.5 To the first thermal pulse

Table 2 presents some variables at the time of the first thermal pulse; the total stellar mass (M_{SAGB}), the ONe core mass (M_{ONe} defined as the point where the abundance of ^{12}C is equal to that of ^{20}Ne) and M_{CO} , the CO core mass, for the all stars studied. The duration of carbon burning is longer in the MONSTAR models and this compensates for the shorter CHeB phase, resulting in the total mass at the first thermal pulse M_{SAGB} converging more closely with the STAREVOL values. Greater discrepancies are found in the more metal-rich models that suffer stronger mass loss. In the majority of the models tabulated, M_{ONe} is greater than the mass of the CO core at carbon ignition (M_{CO_i}). The lowest mass SAGB stars are the exceptions. As they have initially ignited carbon so violently, the carbon content in these outer layers was depleted enough that secondary C-flashes near the H–He boundary will not occur. Close agreement is found between the two main code results, with an average of $\approx 0.04 M_{\odot}$ difference in the M_{ONe} and M_{CO} . The discrepancy in the core masses does not stem from any difference in the carbon burning behaviour, but is simply due to more rapid helium burning, during both the contraction phase and carbon burning itself, in MONSTAR. This always results in more massive stellar cores than those found by STAREVOL.

When considering the further evolution of these stellar models and their ultimate fate, the CO core mass is of vital importance. At the cessation of carbon burning, the core mass differences correspond to approximately $0.2 M_{\odot}$ difference in initial stellar mass.

6 CONCLUSIONS AND FUTURE WORK

Careful tests of the spatial and temporal resolution have confirmed that the carbon burning phase weakly depends on the spatial resolution but that inadequate temporal resolution alters the behaviour of the convective zones. An unexpected result is the fine temporal resolution required during the contraction phase prior to carbon ignition. The time-steps in this phase have to be less than ≈ 2000 yr for consistent results. We emphasize again the need for relatively small time-steps when calculating the evolution of SAGB stars.

With the consistently comparable results between STAREVOL and MONSTAR for stars with the same core mass, we are confident that our nuclear energy generation treatment of the carbon burning is appropriate. We have used one reaction to simulate the carbon burning network and have shown this performs extremely well over a substantial metallicity and mass range when compared to a full network. The benefit is computational time savings with minimal loss in accuracy. The minimum initial mass of star which ignites carbon M_{up} was found to agree within $0.2 M_{\odot}$ between the two codes over the entire metallicity range.

We also report the existence of stellar models where carbon burning is aborted. Such models, close to the M_{up} limit, leave the star with a CO core surrounded by a relatively thick ($0.2\text{--}0.3 M_{\odot}$) shell of partially burnt carbon material.

In conclusion, we find excellent agreement between MONSTAR and STAREVOL for the entirety of stellar evolution until the first thermal pulse. The thermally pulsing phase of evolution and yield production with varying input physics will be described in detail in forthcoming papers in this series.

ACKNOWLEDGMENTS

CLD was supported by a Dean's Postgraduate Research Scholarship from Monash University. LS is an FNRS research scientist. We thank Ross Church for his careful reading of the manuscript. This research was supported under Australian Research Council's Discovery Projects funding scheme (project number DP0877317), by the Communauté française de Belgique – Actions de Recherche Concertées, and by the Spanish Ministry of Education Jose Castillejo grant JC00139. ‘There is as much difference between us and ourselves as between us and others.’ Michel de Montaigne, 1580.

REFERENCES

Angulo C. et al., 1999, *Nucl. Phys. A*, 656, 3
Blöcker T., 1995, *A&A*, 297, 727

- Campbell S. C., 2007, PhD thesis, Monash University
Campbell S. W., Lattanzio J. C., 2008, *A&A*, 490, 769
Cannon R. C., 1993, *MNRAS*, 263, 817
Caughlan G. R., Fowler W. A., 1988, *At. Data Nucl. Data Tables*, 40, 283
Eldridge J. J., Tout C. A., 2004, *Mem. Soc. Astron. Ital.*, 75, 694
Ferguson J. W., Alexander D. R., Allard F., Barman T., Bodnarik J. G., Hauschildt P. H., Heffner-Wong A., Tamanai A., 2005, *ApJ*, 623, 585
Frost C. A., Lattanzio J. C., 1996, *ApJ*, 473, 383
García-Berro E., Iben I., 1994, *ApJ*, 434, 306
García-Berro E., Ritossa C., Iben I. J., 1997, *ApJ*, 485, 765
Gil-Pons P., García-Berro E., 2002, *A&A*, 396, 589
Gil-Pons P., Suda T., Fujimoto M. Y., García-Berro E., 2005, *A&A*, 433, 1037
Gil-Pons P., Gutiérrez J., García-Berro E., 2007, *A&A*, 464, 667
Girardi L., Bressan A., Bertelli G., Chiosi C., 2000, *A&AS*, 141, 371
Graboske H. C., Dewitt H. E., Grossman A. S., Cooper M. S., 1973, *ApJ*, 181, 457
Grevesse N., Noels A., Sauval A. J., 1996, in Holt S. S., Sonneborn G., eds, *ASP Conf. Ser. Vol. 99. Cosmic Abundances, Standard Abundances*. Astron. Soc. Pac., San Francisco, p. 117
Heger A., Langer N., Woosley S. E., 2000, *ApJ*, 528, 368
Herwig F., 2000, *A&A*, 360, 952
Iben I. J., Ritossa C., García-Berro E., 1997, *ApJ*, 489, 772
Iglesias C. A., Rogers F. J., 1996, *ApJ*, 464, 943
Itoh N., Hayashi H., Nishikawa A., Kohyama Y., 1996, *ApJS*, 102, 411
Karakas A., Lattanzio J. C., 2007, *Publ. Astron. Soc. Aust.*, 24, 103
Langer N., 1998, *A&A*, 329, 551
Lattanzio J. C., 1986, *ApJ*, 311, 708
Lugaro M., Ugalde C., Karakas A. I., Görres J., Wiescher M., Lattanzio J. C., Cannon R. C., 2004, *ApJ*, 615, 934
Nomoto K., 1984, *ApJ*, 277, 791
Poelarends A. J. T., Herwig F., Langer N., Heger A., 2008, *ApJ*, 675, 614
Pols O. R., Tout C. A., Eggleton P. P., Han Z., 1995, *MNRAS*, 274, 964
Ritossa C., García-Berro E., Iben I. J., 1996, *ApJ*, 460, 489
Ritossa C., García-Berro E., Iben I. J., 1999, *ApJ*, 515, 381
Schröder K.-P., Cuntz M., 2005, *ApJ*, 630, L73
Siess L., 2006a, in Montmerle T., Kahane C., eds, *EAS Publications Series*, Vol. 19, *Evolution of massive AGB stars*. EDP Sciences, Les Ulis, p. 103
Siess L., 2006b, *A&A*, 448, 717
Siess L., 2007, *A&A*, 476, 893
Straniero O., Domínguez I., Imbriani G., Piersanti L., 2003, *ApJ*, 583, 878
Timmes F. X., Woosley S. E., Taam R. E., 1994, *ApJ*, 420, 348
Vassiliadis E., Wood P. R., 1993, *ApJ*, 413, 641

This paper has been typeset from a $\text{\TeX}/\text{\LaTeX}$ file prepared by the author.